

OXIDE BASED MAGNETIC NANOCRYSTALS FOR
HIGH-FREQUENCY AND HIGH-ENERGY
PRODUCT APPLICATIONS

A Dissertation
Submitted to
the Temple University Graduate Board

In Partial Fulfillment
of the Requirements for the Degree
MASTERS OF SCIENCE
In
MECHANICAL ENGINEERING

By
Ketan Patel
Diploma Date: August 2017

Examining Committee Members:

Dr. Shenqiang Ren, Department of Mechanical Engineering
Dr. Fei Ren, Department of Mechanical Engineering
Dr. Jie Yin, Department of Mechanical Engineering

ABSTRACT

Magnets play a major role in our rapidly developing world of technology. Electric motors and generators, transformers, data storage devices, MRI machines, cellphones, and NMR are some of the many applications for magnets. However, almost all the magnets currently being used have rare-earth heavy metals in them. Despite their high-energy product, the presence of rare-earth metals increases the cost significantly. Also, the processes involved in the mining of rare-earth metals are hazardous to the environment, and to all life forms. In the past few decades, oxide based magnets have gained a lot of attention as potential replacements for the rare-earth magnets.

Oxide based magnetic nanocrystals are attracting a lot of attention as a potential replacement for rare-earth magnets. They are stable in ambient condition and their manufacturing cost is very low when compared to the rare-earth magnets. My work deals with the synthesis of core-shell magnetic structure for high frequency applications (Chapter 1) and the synthesis of high energy product magnetic nanocrystals (Chapter 2) and the synthesis of soft magnetic nanocrystals for high frequency measurement. NiZn ferrite, a soft oxide based magnet cannot be directly implied at high frequencies as they fail at the frequency which over the MHz range. On the other hand, BaZn ferrite is a Y-type magnet, which is robust at higher frequencies. Therefore, using the latter magnet as a protective shell for core material, made of former magnet, enables us to manufacture a cheap solution to the rare-earth magnets used in our cell phones and other devices that work on high frequency signals. On the other hand, successful coating of a very soft magnetic material on a hard-magnetic core increases the total energy product of the magnetic composite, which enhances its versatility.

ACKNOWLEDGMENT

Firstly, I would like thank my thesis advisor and my mentor, Dr. Shenqiang Ren, Department of Mechanical Engineering, Temple University, for his tremendous support towards the project and other aspects of the graduate school. Having a mentor like him served as a great morale booster in times when I was left with no idea how of carrying the project forward. In addition, as I worked on the project, I got the opportunity of learning several research techniques from him, which have made me a better researcher. Apart from the project, he always kept his doors open for me whenever I was in a need of any moral support or needed an advice regarding the classes I have taken. Also, I got an amazing opportunity to give a research presentation at one of the conferences of the Materials Research Society in Boston.

I would also like to acknowledge Dr. Fei Ren and Dr. Jie Yin, Department of Mechanical Engineering, Temple University, for becoming a part of the committee for my thesis proposal and defense. The entire work and effort would have been incomplete otherwise. Also, their positive assessment of my proposal further guided me to the completion of the project.

Furthermore, I would like to thank my lab mates, Dr. Wei Zhang (post doc.) and Dr. Zhuolei Zhang (post doc.) for their assistance in collecting the data and understanding some complex concepts of the magnetism. Also, their tips for carrying out the research made my work significantly easier.

Last but not the least; I would like express my deepest gratitude to my parents, my sister, my girlfriend and my friends for their love, support and encouragement for me during my masters in a foreign country. Without their support, this journey would not have been easier. Thank you.

Author

Ketan Patel

TABLE OF CONTENTS

	Page
ABSTRACT	ii
ACKNOWLEDGMENT.....	iii
LIST OF FIGURES	v
LIST OF TABLES.....	vi
INTRODUCTION	vii
CHAPTER	
1. CORE/SHELL MAGNETIC NANO-COMPOSITES FOR HIGH- FREQUENCY APPLICATIONS.....	1
1.1 Selection of The Materials.....	1
1.2 Synthesis	2
1.3 Results and Discussion.....	4
2. OXIDE BASED CORE/SHELL MAGNETIC COMPOSITE FOR HIGH-ENERGY PRODUCT APPLICATIONS.....	8
2.1 Selection of The Materials.....	8
2.2 Maximum Energy Density (BH_{max})	8
2.3 Synthesis	9
2.4 Results and Discussion.....	10
CONCLUSIONS	13
REFERENCES	14

LIST OF FIGURES

	Page
Figure 1 (types of magnets and their market share; before and after alignment magnetic domains).....	xi
Figure 2 (crystal structure of Sr-ferrite and Ba/Zn-ferrite).....	1
Figure 3 (TEM images of the core-shell magnetic composite).....	4
Figure 4 (shell thickness dependent TEM and EDS images).....	5
Figure 5 (shell thickness dependent XRD images).....	5
Figure 6 (shell thickness dependent hysteresis loop and resistance measurements).....	6
Figure 7 (easy magnetic axis and hard magnetic axis of the core/shell composite).....	6
Figure 8 (sintering temperature dependent hysteresis loop and resistivity measurement).....	7
Figure 9 (curves for BHmax calculation).....	9
Figure 10 (TEM, XRD and EDS images of Sr-ferrite and FeCo as core /shell composites).....	11
Figure 11 (comparison of the magnetic properties among pure Sr-ferrite, pure FeCo and composites with various shell thickness).....	12

LIST OF TABLES

	Page
Table 1 (represents the coercivity and BH_{\max} of the samples ranging from 0 to 40 wt% of FeCo shell).....	12

INTRODUCTION

Magnetism is one of the fundamental phenomenon observed in the nature and we are surrounded by the magnetic fields. Before the age of technology, the magnetic fields, from the earth's core, only protected us from the harmful solar radiation. But, as humans progressed and learned the concepts of electricity and magnetism, we started utilizes magnetism from magnetic materials to our own benefits. This led to a revolution in the inventions of many electro-magnetic devices that have parts of lives now. Similar to mass and electrons, every material has an intrinsic magnetic moment that originates from the spin of the electrons, which is the source of the magnetism. However, in order to have a net magnet ic moment there has to be half filled orbitals and that is why there are not many magnetic materials found in nature. But, immense amount of scientific research has now enabled us to synthesize our own magnets via various procedures. Furthermore, magnets can be broadly classified into two groups, hard and soft[1, 2]. Magnets that require a lot of energy to switch their polarity are considered hard and are used for applications like motors and generators. On the other hand, the magnets that switch their polarities with only a tiny amount energy are considered as soft and are applicable in cellpho ne, inductors, transformers and other electromagnetic devices. To dig a little deeper, the hardness and softness of a magnet depends on its domains (figure 1), which is a region of atoms with their magnet ic moments in the aligned in the same direction. Furthermore, we use a terminology, coercivity, as a measure of hardness/softness of a magnetic material. Larger the coercivity, harder the magnet and vice versa. Larger domains require larger energy to flip to complete opposite direction and smaller domains. Domains are usually randomly ordered that gives rise to a zero net-magnetic field. However, a sufficiently strong magnetic field can align all the domains in one direction and reveal the magnet ic properties of the material[1-7]. The maximum magnetic field obtained after the alignment of all the domains is what we cal as "saturation magnetization". Another important parameter to be considered is the permeability of a material. Permeability is the tendency of a material to be magnetized. This is a crucial factor to consider because magnets with higher permeability more efficient while transmitt ing any received signal to the system. Currently, there five different types of magnets being used in the market, which include magnetic alloys of Aluminum, Nickel and Cobalt, ferrite based magnets, rare- earth metals based magnets and combinations of these magnets. Furthermore, looking at the graph in figure 1 shows the distribution of the market share (year 2007) of the various kinds of the magnets. The data give an idea about the inclination of the human interest towards the rare-earth magnets[8-10], [36].

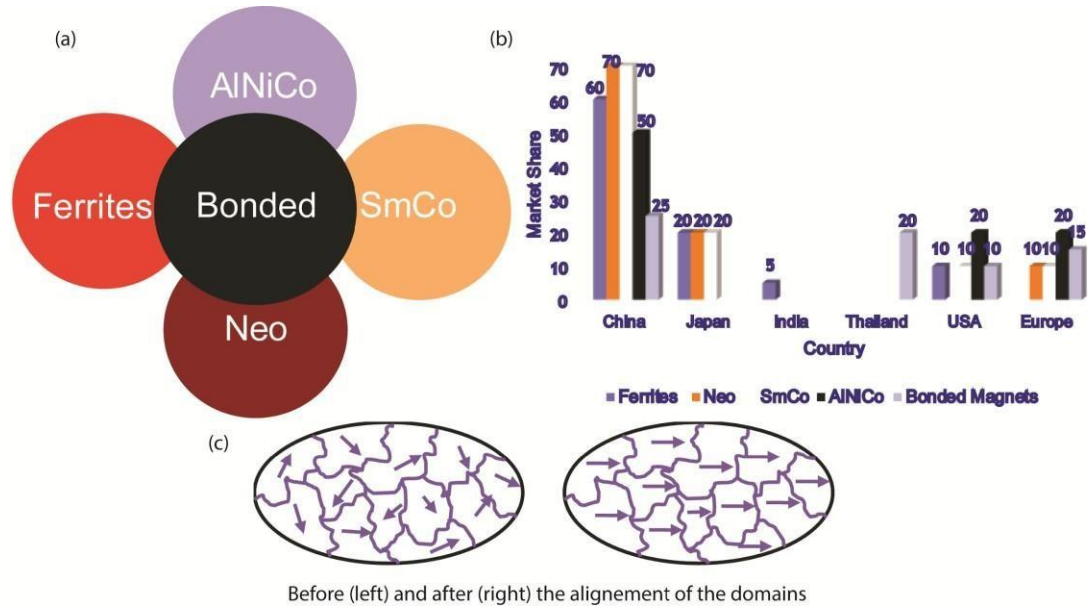


Figure 1: a. types of magnets in the market, b. marketshare of the magnets from 2007, c. representation of magnetic domains before and after their alignment.

The rapid advancement in the technology has led numerous devices to miniaturize, such as cell phones, computers, electromagnetic devices, etc., with significant increase in their performances. Also, the miniaturization happens with an increase in the performance of the devices as well. Therefore the demand for better magnets increases with every new technology. Due to this, the demand for rare-earth metals based magnets skyrocketed, which also increased the mining of the rare-earth metals. The mining of rare-earth metals are hazardous to all live forms as they create several socio-economic problems and the waste product from the mining pollutes land, water and air killing countless living organisms. Therefore, there is an urgent demand for a feasible and an eco-friendly solution to these problems [11-21]. Oxide based magnets, due to their stability in the ambient conditions and low cost, have been attracting researchers to find ways to making them comparable to that of the rare-earth metal magnets[22]. Therefore, to address these challenges, since past few decades, numerous works and studies and have been conducted. Some of those works feature Manganese (Mn) based magnetic alloys, where Mn is incorporated with other transition metals to form magnetically active alloys[23-26]. Some other work have dealt with enhancing the energy product of the oxide based magnets where researchers have attempted to generate high magneto-crystalline anisotropy[9, 22]. Additionally, Fe and Co have been utilized extensively for manufacturing the rare-earth free magnets. From Fe and Co alloys to making iron oxide core/shell, constant efforts have been made for seeking the possible solution to

replace the rare-earth elements from the market[9, 22, 27-31]. In fact, newer techniques such as computational modellings are also been used to do so as well. All these effort towards a cleaner and safer environment motivated me to carry on my project towards the replacement of the rare-earth metal magnets with the transition metal magnets.

My work consists of two halves, in which, I study two different methods of enhancing oxide-based magnets so that they can potentially be utilized as a replacement for the rare-earth metal magnets. First half of my work deals with making an oxide based magnet, $\text{NiZnFe}_2\text{O}_4$ (NiZn-ferrite), to be safely at higher frequencies by concealing it inside a robust magnetic shell, $\text{Ba}_2\text{Zn}_2\text{Fe}_{12}\text{O}_{22}$ (BaZn- ferrite), without significantly effecting the overall magnetism. On the other hand, for my second half of my work, I attempted to enhance the energy product of another oxide-based hard magnet, $\text{SrFe}_{12}\text{O}_{19}$ (SFO), by coating it by a soft magnet, FeCo, on it so that the final composite could be used for applications such as electric motor and generator. While carrying out my work, I had to utilize several research techniques such as, Transmission Electron Microscope (TEM), Scanning Electron Microscope (SEM), X-Ray Diffractometer (XRD), Vibrating Sample Magnetometer (VSM) and Energy Dispersive Spectroscopy (EDS).

CHAPTER 1

CORE/SHELL MAGNETIC NANO-COMPOSITES FOR HIGH-FREQUENCY APPLICATIONS

1.1 Selection of The Materials

This work focuses towards finding a feasible replacement for the rare-earth element magnets for the high frequency applications. The magnets that can be applicable in these applications need to be soft in nature with saturation magnetization (M_s) as large as possible, low cost and environmentally friendly. Hence, oxide based, spinel structured, magnets could be an ideal choice. However, a drawback of these magnets is that they fail at high frequencies. Therefore, we need to conceal them inside a shell, which needs to be robust at higher frequency. Also, proper care needs to be taken while preparing the shell so that it does not degrade the magnetic performance of the entire composite. Hence, a very well known Y-type hexagonal BaZn-ferrite is a reasonable choice for the given purpose. Figure 2 gives us an idea of the crystal structure of the respective materials [32, 33].

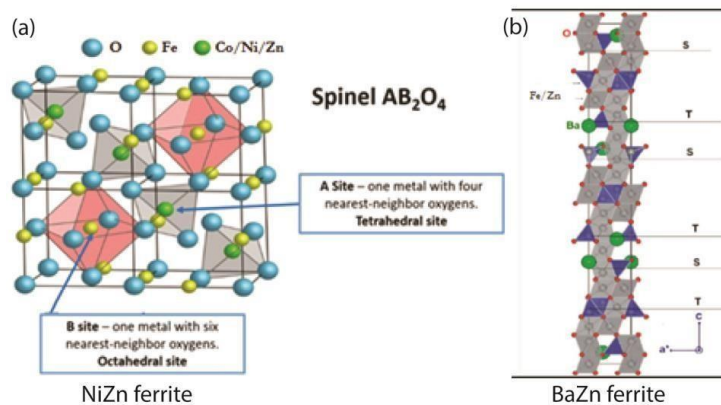


Figure 2 a. crystal structure of NiZn ferrite, b. crystal structure of BaZn ferrite

1.2 Synthesis

Both the soft magnet (core) and the hard magnet (shell) were synthesized by different synthetic procedure. To synthesis the soft magnet (core), NiZnFe₂O₄ (NiZn-ferrite), I followed a solution based approach, which is called as colloidal based solution synthesis[34]. In this technique, depending on the decomposition temperature of the metal precursors and their decomposition rates, the metal precursors are either mixed in the same reaction flask or different reaction flasks with the solvent, a ligand and an oxidizing agent. The purpose of using a ligand is to restrict the particle growth to the nanometer range, ideally to their domain size, so that we obtain maximum magnetism from the particles. In addition, the reaction takes place in an inert environment, in the absence of air and moisture and thus we need an oxidizing agent to supply the metal cations enough oxygen molecules in order to form the desired final product. There are three major advantages of letting the reaction take place in an inert environment; firstly, it eliminates any potential contamination from the particles present in the air, secondly, the reaction takes place at a temperature much higher than the boiling point of the water and therefore, it is essential that there is no water present in the reaction flask, thirdly, we can control the amount of oxidizing agent that we add in the reaction and this allows us to control the quality of the final product. The reaction procedure is as follows: in a 3-neck flask appropriate moles of Ni, Zn and Fe precursors are added (I used only one flask because after several preliminary reactions it was evident that all the three metal precursors have similar rate of decomposition) and mixed with right volumes of the solvent (1-Octadecene), the ligand (Oleyamine) and the oxidizing agent (Oleic Acid). The mixture is then allowed to mix properly on a magnetic stirrer for 5 minutes. The reaction flask is then properly sealed and connected to a Standard Schlenk-line and is subjected to at least three cycles of vacuum and nitrogen purge so that the flask is free of air and moisture. After that, the temperature of the flask is slowly raised to ~120 °C and three more cycles of the vacuum and nitrogen purge were done. This step ensures that all the water molecules from the metal precursors are removed. Finally, the temperature of the reaction flask is slowly increased (3.5 °C per minute) to ~320 °C and is maintained for 2 hours. Lower temperatures fail to supply enough energy for the particles to form and lesser time is not long enough for the desired size of the particles. The final product also depends on the rate of increase of the reaction temperature. A faster rate than 3.5 °C per minute does not form the appropriate particles and the slower rate potentially forms iron oxide before reaching

the reaction temperature as it takes about 3 hours to reach ~ 320 °C at an increment of ~ 1 °C per min. Finally, after the reaction is done, the flask is allowed to cool down naturally to the room temperature and it is then when the solution is washed by adding Acetone (bad solvent) and Toluene (good solvent) in *via* centrifuge to collect the particles. The as-synthesized particles are permanent magnets; however, their crystallinity can still be increased, in order to obtain maximum magnetization. To do so we sinter the particles in a box-furnace at 1000 °C for 4 hours.

To synthesize the hard magnet (shell), $\text{Ba}_2\text{Zn}_2\text{Fe}_{12}\text{O}_{22}$ (BaZn-ferrite) I utilized a very well-known and widely used synthesis technique called as “hydrothermal process”. There is a great advantage in using this synthesis technique. Most of the commonly used barium salts do not dissolve in the organic solvents but readily dissolve in water. Also, I can add my already synthesized core magnets in the autoclave, which will act as nucleation site for the BaZn-ferrite particles to form, thus also making the formation of the shell much easier. The procedure is as follows: appropriate amount of Ba, Zn and Fe precursors are mixed with deionized (DI) water in the autoclave in the presence of the previously synthesized and sintered NiZn-ferrite particles. We must make sure that the DI water is not more than 50% of the volume of the autoclave for safety reasons. After properly mixing all the precursors and the core magnet in the water, we properly seal the autoclave and put in an oven at ~ 150 °C for over a night. The excess vapor pressure built in the autoclave forces the Ba, Zn and Fe particles to bond and form the Y-type hexagonal ferrite on top of the NiZn ferrite particles. The formation of Y-type hexagonal ferrites is dictated by the appropriate molar ratios of the metal precursors. We do not need any ligands and oxidizing agents in this process. This is because majority of the BaZn-ferrite particles grown only on the surface of the NiZn-ferrite. Also, the required oxygen is supplied by the organic part of the Fe precursor and the air present in the autoclave. After letting the reaction to take place for overnight the solution is washed with DI water and the particles are collected and sintered again at 500 °C for 2 hours to enhance the crystallinity of the shell.

1.3 Results and Discussion

The most important step, after the synthesis, is to ascertain the success of the synthesis. In other words, we need to make sure that the synthesis has produced the desired outcome. To do so, state-of-the-art research equipment such as, TEM, XRD and SEM are utilized. In addition, there are two different ways to coat the shell on the core. First, coating the shell on a non-sintered shell and second, coating the shell on the sintered shell. The latter turned out to be the better method and it is evident from the figure 3. Looking at the TEM images, we see that the particles of the shell magnet were not able to get coated on the non-sintered core. This was due to the fact that the surface of the non-sintered core magnet has organic ligands attached. These organic ligands do not let the particles of the shell magnet to deposit on the surface of the core magnet because the

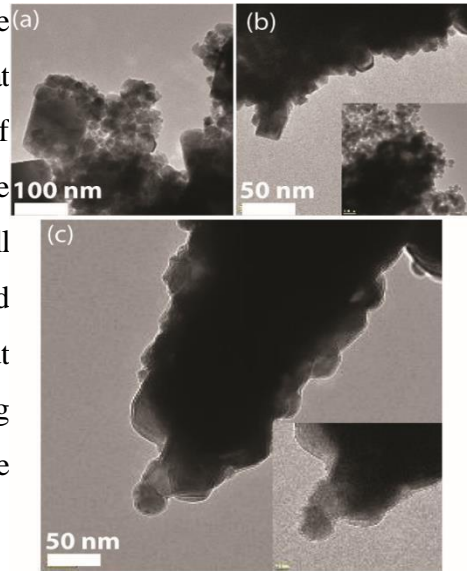


Figure 3. sintered shell coated with BaZn ferrite (BaZn ferrite particles around core), b. non-sintered core coated with BaZn ferrite (BaZn ferrite particle nowhere around the core), c. "a" after sintering (formation of robust shell around the core)

coating process takes place in DI water. Also, we can see the formation of the shell on the core after sintering the "sintered-core" sample. Furthermore, the figure 4 assists in assessing the increased shell thickness on the core. We can observe the distinction between the edges of the core particles (figure 4 a) and the coated ones suggesting the presence of an additional material on the core. Also, as the shell gets thicker, the center of the particles keeps getting darker, which further points towards a change in the concentration of the shell. Moreover, the EDS (figure 4 b) mapping from the 10 wt% sample reveals the presence of nickel, zinc, iron, oxygen and barium in it, thus suggesting towards a successful synthesis. After acquiring the visual confirmation, we need to gather evidence for the proper chemical composition of the sample. Hence, we subject our sample to the X-rays and study the spectra obtained from the interactions of the x-rays and the sample. We see, from figure 5, that there are considerable changes in the peaks as the concentration of the shell increases. From the spectrum with 0 wt% of the shell, we determine that the composition of the core is $\text{NiZnFe}_2\text{O}_4$. Also, as the thickness of the shell increases, we observe an increase in the peak at around $2\theta \sim 42^\circ$, suggesting it to be the peak for the shell, $\text{Ba}_2\text{Zn}_2\text{Fe}_{12}\text{O}_{22}$.

Since we are incorporating two different magnets into each other, an interest arises to study how this incorporation affects the final composite. Hence, we study the magnetism in our samples with the aid of VSM. This study is important also because the final product needs to be as soft-magnet as possible and its saturation magnetization (M_s) needs to be as large as it can be. Figure 6a shows the compiled VSM curve for the samples from 0 wt% shell to 50 wt% shell. The M_s of pure core is around 40 emu/g and the change in M_s of the

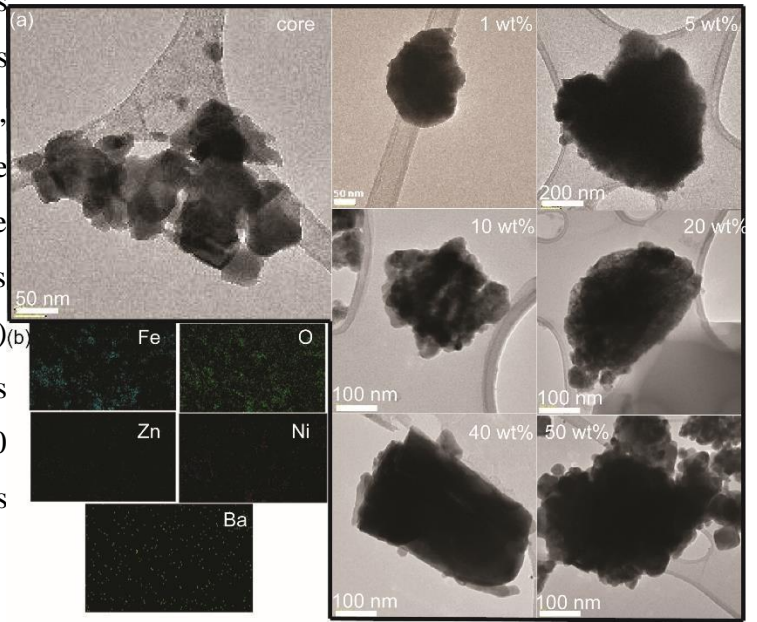


Figure 4. NiZn ferrite (core) with increasing shell thickness, b. EDS mapping of the 10 wt % shell sample

composite, after the incorporation the shell, is roughly by $\sim 12\%$. However, there is a notable change in the coercivity of the composite. We observe a steady increase in the coercivity of the composite as the shell thickness increase. This is because the shell is a Y-type hexagonal ferrite that is a hard magnet. Furthermore, to be able to be used in an electro-magnetic device, the final composite needs to work at higher frequencies without failing. Therefore, it is essential to

measure the resistance of the samples. Hence, respective devices were prepared for all the samples and each one them was tested with an impedance-measuring device. Figure 6b shows the detailed spectra of all the samples ranging from 0 wt% shell o 50 wt% shell. We observe that the resistance considerably increases from 5M ohms to about 5G ohms just by adding 1 wt% of the shell. Further addition of the shell shows a steady, but a very small, increment in the resistance of the composite, which start to degrade after further addition of the shell past 20 wt%. This indicates that 20 wt% shell is the optimum sample in terms of

resistance of the composite at high frequency. However, 1 wt% sample has much lower coercivity, which is a key factor in this

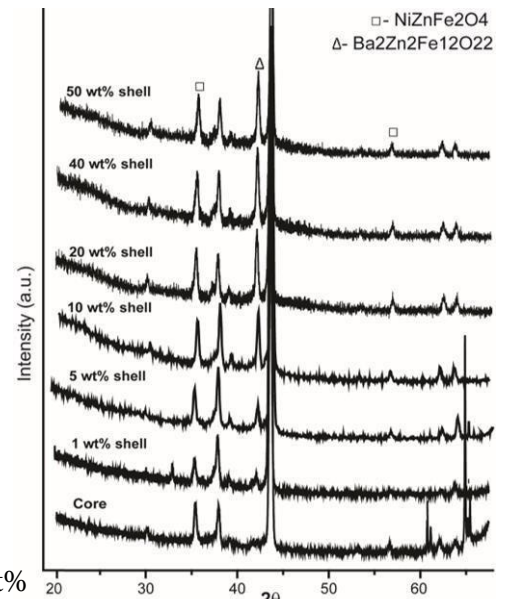


Figure 5. Shell thickness dependent XRD spectra of the core/shell magnetic structure

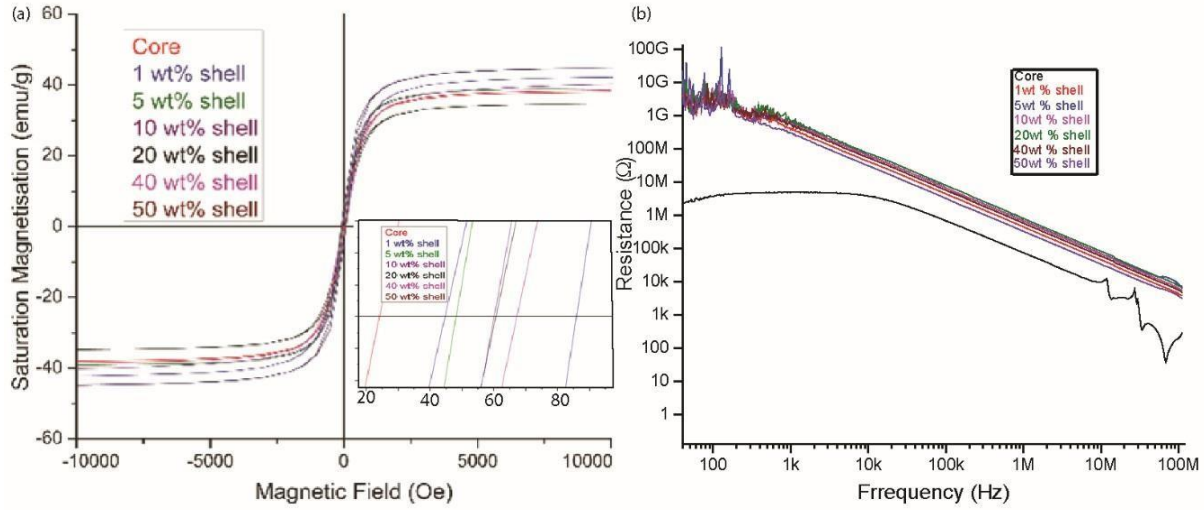


Figure 6 a. shell thickness dependent MH loop, b. shell thickness dependent high-frequency resistance measurement

work, with respect to the 20 wt% sample without showing any considerable difference in the resistivity. Therefore, the sample with just 1 wt% shell is deemed as the better composite than any other. Another key factor to note is the permeability of the sample. As stated above, permeability of a material is its tendency to be magnetized when subjected to an external magnetic field. In this work, permeability needs to be studied to make sure that the magnet in the electro-magnetic device transfers the signals into the system efficiently. To do so, I analyzed the easy and the hard

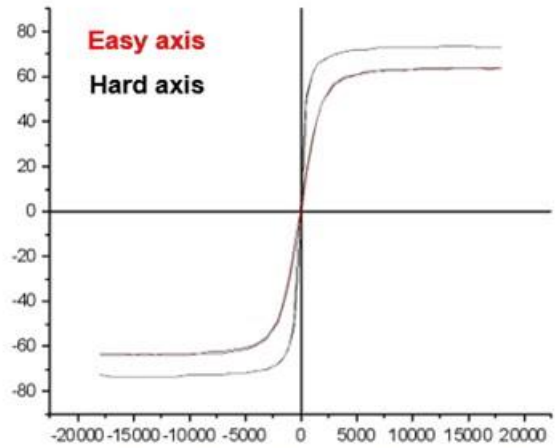


Figure 7. Representation of easy and hard axis of the core/shell magnetic composite via MH loop

axes of all samples (figure 7). Studying easy and hard axes gives us an idea of the permeability of the material. Furthermore, using the data from the easy and hard and using the following equation gives the permeability of the desired samples.

$$\mu = \frac{1 + 4\pi\gamma^2 Ms \{ (4\pi Ms + Hk) (1 + \alpha^2) [\omega\sigma^2 (1 + \alpha^2) - \omega^2] + (4\pi Ms + 2Hk) (\alpha\omega)^2 \}}{[\omega\sigma^2(1 + \alpha^2) - \omega^2]^2 + [\alpha\omega\gamma(4\pi Ms + 2Hk)]^2} \quad (1)$$

In addition, sintering temperature affects the crystallinity of the composite significantly by further increasing their crystallinity. Therefore, I also studied the effect of the sintering temperature of on the

samples. However, for this study I chose the optimum sample, 1wt % shell and the 10 wt% shell sample to have a comparative analysis. Figure 8 shows the sintering temperature dependent magnetism study and high frequency resistance study for the two samples. It is very interesting to note that the 1 wt% shell sample, sintered at 650 °C, turns out to be the best performing sample. Also, at higher sintering temperature the crystallinity of the composite increase, which in turns increase the coercivity of the shell magnet and the overall coercivity of the composite as well. Looking at the resistivity data of the same sintering temperature dependent sample, we fo not observe any considerable changes in the data. Therefore, from all these data, the core/shell magnetic composite with 1 wt% shell and sintered at 650 °C turned out to be the best performing sample.

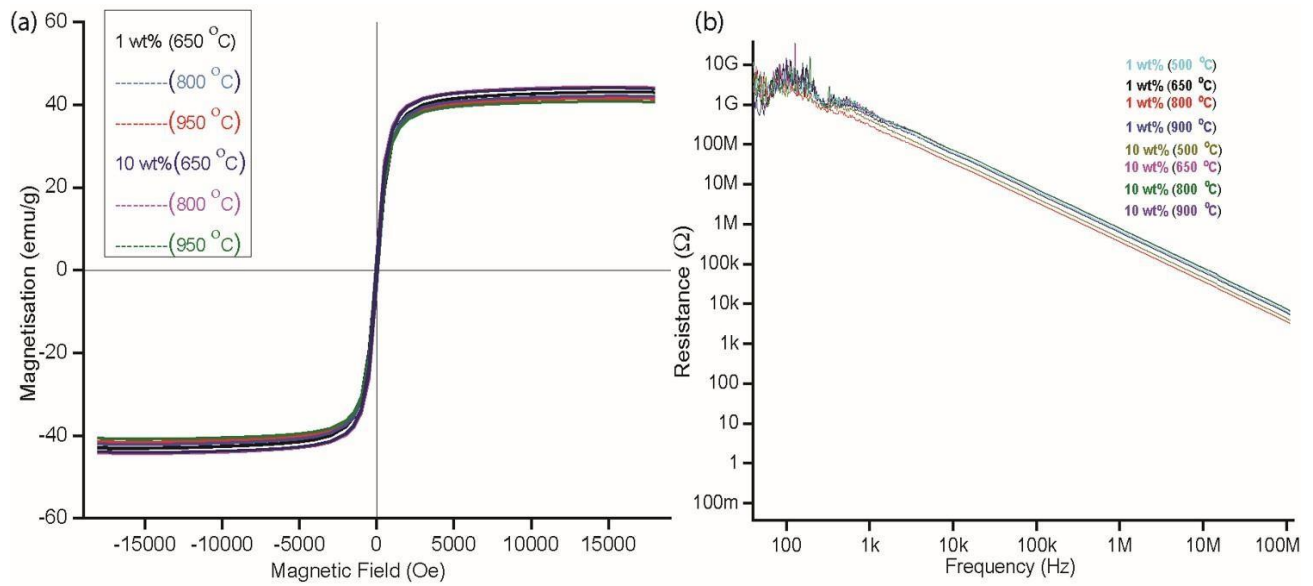


Figure 8a. Sintering temperature dependent MH loop for 1 wt% and 10 wt% shell samples, b. Sintering temperature dependent resistance measurements for 1 wt% and 10 wt% shell samples.

CHAPTER 2

OXIDE BASED CORE/SHELL MAGNETIC COMPOSITE FOR HIGH-ENERGY PRODUCT APPLICATIONS

2.1 Selection of The Materials

This work was done keeping the goal to improve the maximum energy product of the traditionally used oxide based hard magnet, Strontium Ferrite (SFO), by incorporating it with a soft magnet[34]. One of the key points to keep in check is to have a good interface between the hard and soft magnet, which will help in giving out the maximum magnetic properties from both magnets. In this work, since we need a soft magnet as a shell, a well-known soft magnetic alloy of Fe and Co, FeCo, was chosen to be the shell material[35]. The idea, here, is to coat the SFO, a M-type hexagonal ferrite, with a cubic structured FeCo in such a way that the final composite has the properties of both the magnets thus increasing the maximum energy density of the composite. Figure xx give an idea of the crystal structure of both the magnets.

2.2 Maximum Energy Density (BH_{max})

Maximum Energy Product or Maximum Energy Density of a magnet is a parameter to assess the grade of a magnet. This, in any way, does not indicate the strength of a magnet. For example, a Neodymium based magnet has BH_{max} equal to 48. In other words, the grade of the Neodymium based magnet is 48. Looking at figure xx shows us the immense difference between the grades of rare-earth based magnets and the ferrite based magnets. Thus, there is a need to enhance the grade of the cheap and environmentally friendly ferrite based magnets.

There are several ways to calculate the BH_{max} of a magnet. First, the largest area under the B

(magnetic flux) vs H (coercivity) of the magnet gives us the BH_{max} of the sample. Another method is by converting the M-H loop of a sample into a B-H loop. Then, the maximum point of the parabola obtained by plotting BH vs H gives the BH_{max} of the given sample. The third method is by using a formula to obtain B from M, which is $B = \mu_0(H + M)$, where M and H are in oersted (Oe). The units of BH_{max} is MGOe (Mega Gauss Oersted). Figure 9 shows the graph between B and H and the parabola between BH and H[37].

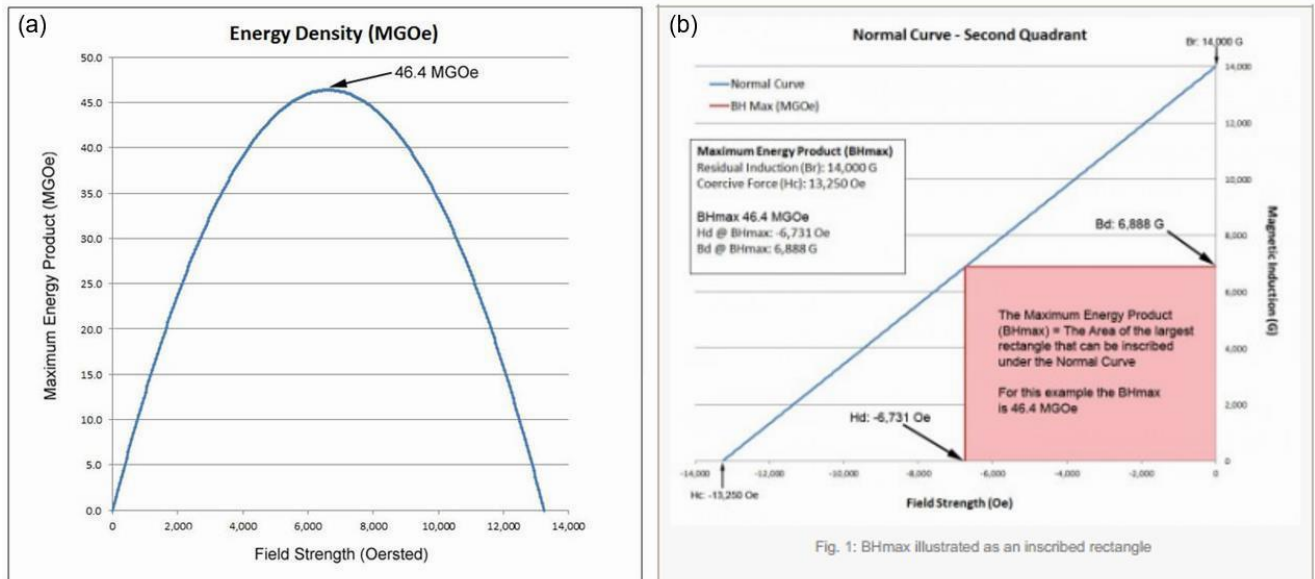


Figure 9. curves to calculate BH_{max} to a given magnet.

2.3 Synthesis

The synthesis of the SFO is exactly same as that of the synthesis of NiZn-ferrite, which has been discussed in section 1.2 with the only difference being in the metal precursor. One key feature of this synthesis technique is that it enables us to use any metal salt, as a precursor to final product, that dissolves in an organic solvent. This feature makes this technique very versatile. Also, after the synthesis, the SFO particles were sintered at 1000 °C for 240 minutes. This is an essential step in order to ensure the proper crystallinity of the SFO particles. Strontium cations are much larger than the voids present in the skeleton made by the iron oxide molecules. On the other hand, the

synthesis of the Fe and Co magnetic alloy involves specific precursors where the metal is in '0' oxidation state, for example metal carbonyls[35]. For Fe the precursor used was $\text{Fe}(\text{CO})_5$ and for the Co it was $\text{Co}_2(\text{CO})_8$. These chemicals are highly unstable and require to be stored in cold areas and in an inert environment, such as a glove box filled with N_2 . The synthesis procedure is as follows: first, a 3-neck flask is filled with appropriate amount of ODE. The flask is then subjected to three cycles of vacuum and N_2 purge. After that, the flask is heat till the temperature reaches $\sim 120^\circ\text{C}$. Then, three more cycles of vacuum and purge is allowed to take place. Once they are done, the flask is then heated again to a temperature around 180°C . Then in a small vial, sufficient volume of ODE is added. The vial is then bubbled with nitrogen for 2 minutes in order to remove the air and moisture from the vial. The vial is then transferred into the glove box and the proper amount of Co precursor is added into the vial and mixed thoroughly. In another vial, proper amount of Fe precursor is added. After that, both the precursors are rapidly injected into the flask, which is maintained a 180°C . Soon after the injection, the temperature of the flask is quickly raised to $\sim 220^\circ\text{C}$. The flask is then maintained at $\sim 220^\circ\text{C}$ for 30 minutes. Then the flask is allowed to cool and the FeCo particles are collected by centrifuging the final solution followed by washing with Acetone and Toluene. The particles are then carefully dried by a steady nitrogen flow and then sintered at 500°C for about 30 minutes in foaming gas (5% H_2 + 95% N_2) environment. For coating of FeCo on SFO, adding SFO in the 3-neck flask with ODE helps Fe and Co to deposit on the surface of the SFO. For further analysis, the sample is stored inside the glovebox as they are very sensitive to air.

2.4 Results and Discussion

The structural characterization of the samples begun by analyzing the samples under TEM. As seen in the figure 10, the shell thickness increase as the wt % of the shell increases. As the shell gets thicker, it becomes more distinct in the images and at 40 wt% it is very clear to see the shell surrounding the core. Furthermore, the distortion in shell is due the fact that the shell always takes the shape of the core. Since the core has been sintered at 1000°C , the nanoscopic particles agglomerate to form larger and distorted particles. Furthermore, studying the samples under SEM

and getting the elemental mapping reveals the presence of Sr, Fe, O, and Co suggesting a proper formation of core-shell. However, it is the data from XRD which backups all the data from TEM and SEM and confirms the chemical composition of the core and shell materials of the composite. In addition, we also see peaks of Co-ferrite, which is due to the oxidation of the FeCo while being exposed to the air.

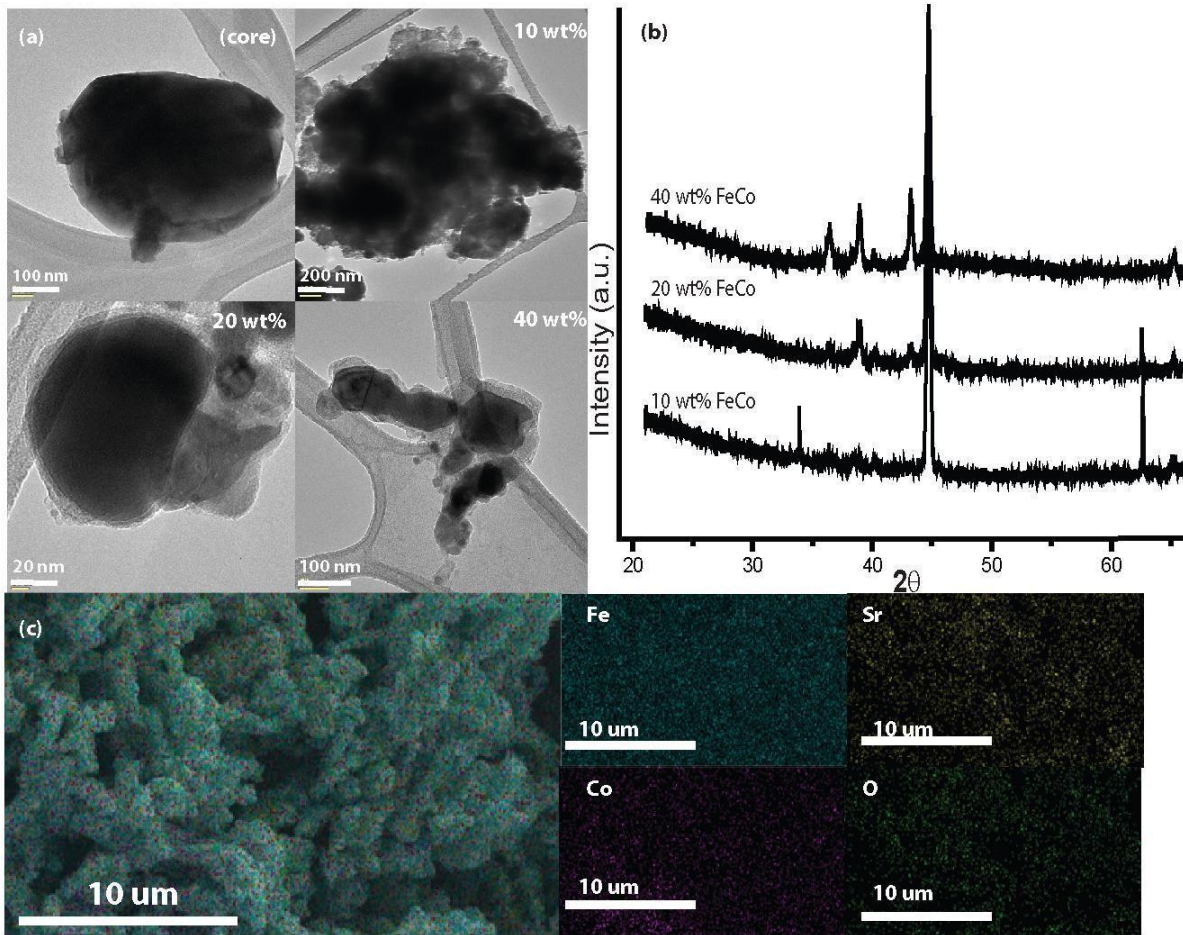


Figure 10a. Shell thickness dependent TEM images of core/shell magnetic complex, b. Shell thickness dependent X-Ray diffraction of the core/shell magnets, c. SEM images and EDS mapping of the 40 wt% shell sample.

After the structural analysis, to measure the magnetic properties of the samples we use VSM to obtain their respective M-H loops. Figure 11 a shows the enormous difference between the magnetic characteristics of SFO and FeCo. Furthermore, figure 11 b shows how the M-H loop changes with respect to the wt % of the shell. Also, the smooth curve indicate a proper interface

between the core and shell. In addition, the data obtained from these graphs help us to calculate their respective energy products. In order to calculate the BHmax for each sample, I used the third method mention above, which involves the formula $B = \mu_0(M + H)$, where H and M are in oersted and μ_0 is the absolute permeability of the medium the material is in. The following table show the BHmax of all the samples.

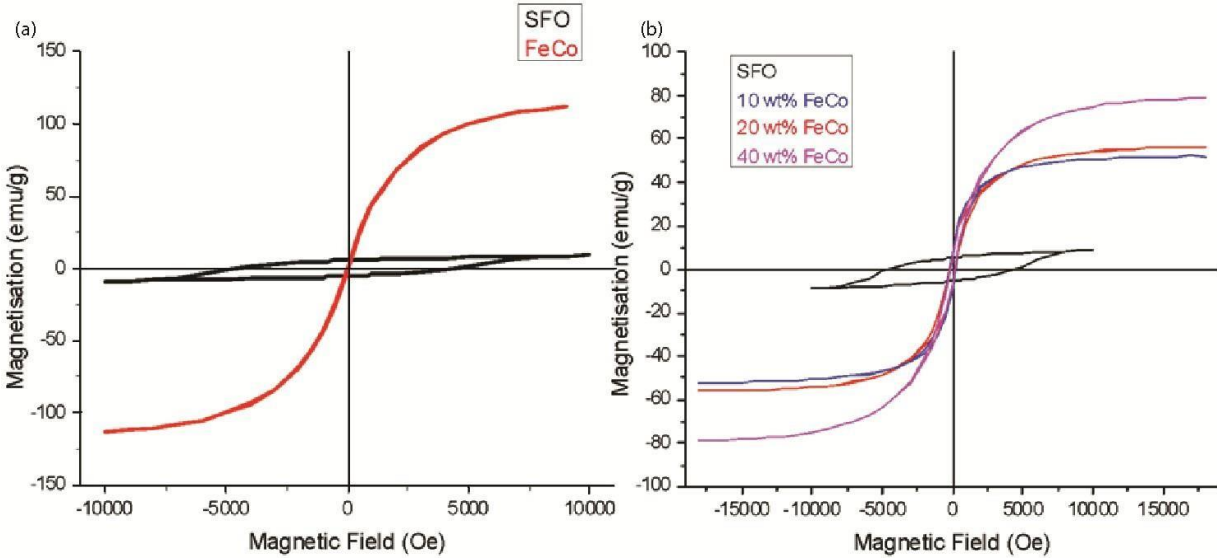


Figure 11a. MH loop of SFO and FeCo, b. shell thickness dependent MH loop of the core/shell magnetic composite.

Sample Number	FeCo wt%	Coercivity (Oe)	BHmax (MGOe)
1	0	5000	.3
2	10	235	.8
3	20	225	.7
4	40	175	.5

Table 1. Represents the coercivity and BHmax of the samples ranging from 0 to 40 wt% of FeCo shell

From table 1, we observe that the BHmax of the sample with no shell has only a .3 MGOe BHmax. However, the BHmax increase with the shell thickness but starts to drop soon after. Therefore, here, the optimum shell thickness is turns out to be no more than 10 wt% of FeCo.

CONCLUSIONS

In first half of this work, I studied a method of protecting an oxide based at higher frequencies without causing much effect on its magnetic properties. That was done coating it with another layer of a magnetic material that is robust at high frequencies. In addition, the composite showed more 1000 times larger resistance at higher frequencies than resistance of the pristine oxide based magnets. Therefore, the work shows the possibility towards utilizing cheaper and eco-friendly magnets in the daily use appliances. On the hand, in my second part of my work, I demonstrated a method of increasing the energy product of a magnet by successfully creating an interface between a hard and soft magnet so that the composite has the properties from both the materials. This is what enhances the final BHmax. For my work the BHmax was increased by a maximum of 166.66%. Furthermore, both of my work can potentially be carried in future for further improvements.

REFERENCES

1. Mahmood, S., S.H. Mahmood, and I. AbuAljarayerh, *Basics of Magnetism*. Hexaferrite Permanent Magnetic Materials. 2016. 1-46.
2. Martins, M. and W. Wurth, *Magnetic properties of supported metal atoms and clusters*. Journal of Physics-Condensed Matter, 2016. **28**(50).
3. Aktas, B., *A survey of nanomagnetism*, in *Nanostructured Magnetic Materials and Their Applications*, D. Shi, et al., Editors. 2002. p. 1-21.
4. Darling, S.B. and S.D. Bader, *A materials chemistry perspective on nanomagnetism*. Journal of Materials Chemistry, 2005. **15**(39): p. 4189-4195.
5. Fischer, P., *Exploring nanoscale magnetism in advanced materials with polarized X-rays*. Materials Science & Engineering R-Reports, 2011. **72**(5): p. 81-95.
6. Hoffmann, A. and H. Schultheiss, *Mesoscale magnetism*. Current Opinion in Solid State & Materials Science, 2015. **19**(4): p. 253-263.
7. Zhou, Y., K. Kanoda, and T.K. Ng, *Quantum spin liquid states*. Reviews of Modern Physics, 2017. **89**(2).
8. Ahn, S., et al., *Analysis of stock prices of mining business*. Physica a-Statistica l Mechanics and Its Applications, 2011. **390**(12): p. 2340-2349.
9. Hwang, H., S. Bae, and C. Lee, *Analysis and Design of a Hybrid Rare-Earth-Free Permanent Magnet Reluctance Machine by Frozen Permeability Method*. Ieee Transactions on Magnetics, 2016. **52**(7).
10. Rollat, A., et al., *Prospective analysis of the flows of certain rare earths in Europe at the 2020 horizon*. Waste Management, 2016. **49**: p. 427-436.
11. Borrego, J., et al., *Effect of acid mine drainage on dissolved rare earth elements geochemistry along a fluvial-estuarine system: the Tinto-Odiel Estuary (SW Spain)*. Hydrology Research, 2012. **43**(3): p. 262-274.
12. Cai, D.J. and Y.K. Rui, *Contents of Rare Earth Elements in Orange from Rare Earth Mining Area of Wuxun, China*. Asian Journal of Chemistry, 2013. **25**(14): p. 8210-8210.
13. Cuvier, A., et al., *Trace elements and Pb isotopes in soils and sediments impacted by uranium mining*. Science of the Total Environment, 2016. **566**: p. 238-249.
14. Ge, J.P., Y.L. Lei, and L.R. Zhao, *China's Rare Earths Supply Forecast in 2025: A Dynamic Computable General Equilibrium Analysis*. Minerals, 2016. **6**(3).
15. Liu, S.H., et al., *The genetic diversity of soil bacteria affected by phytoremediation in a typical barren rare earth mined site of South China*. Springerplus, 2016. **5**.

16. Packey, D.J. and D. Kingsnorth, *The impact of unregulated ionic clay rare earth mining in China*. Resources Policy, 2016. **48**: p. 112-116.
17. Pagano, G., et al., *Rare earth elements in human and animal health: State of art and research priorities*. Environmental Research, 2015. **142**: p. 215-220.
18. Soltani, N., et al., *Geochemistry of Trace Metals and Rare Earth Elements in Stream Water, Stream Sediments and Acid Mine Drainage from Darrehzar Copper Mine, Kerman, Iran*. Water Quality Exposure and Health, 2014. **6**(3): p. 97-114.
19. Sporleder, D., et al., *FATE OF ENVIRONMENTAL RELEVANT ELEMENTS IN AN ISOLATED RIVER CATCHMENT AFFECTED BY ACID MINE DRAINAGE*, in *Water Resources, Forest, Marine and Ocean Ecosystems Conference Proceedings, Sgem 2016, Vol Iii*. 2016. p. 129- 136.
20. Xu, C.Y., et al., *Research of Soil Nitrides Migration Characteristics in Ion-type Rare Earth*. 2016 International Conference on Environmental Science and Engineering (Ese 2016), 2016: p. 798-806.
21. Yang, Q.H., et al., *Heavy Metal Enrichment and Edible Safety of Two Vegetables in Rare Earth Tailings*. 2016 International Conference on Environmental Science and Engineering (Ese 2016), 2016: p. 710-721.
22. Lottini, E., et al., *Strongly Exchange Coupled Core/Shell Nanoparticles with High Magnetic Anisotropy: A Strategy toward Rare-Earth-Free Permanent Magnets*. Chemistry of Materials, 2016. **28**(12): p. 4214-4222.
23. Feng, J.N., et al., *Magnetic Properties and Coercivity of MnGa Films Deposited on Different Substrates*. Journal of Materials Science & Technology, 2017. **33**(3): p. 291-294.
24. Ono, A., et al., *Ultrathin films of polycrystalline MnGa alloy with perpendicular magnetic anisotropy*. Applied Physics Express, 2017. **10**(2).
25. Shen, J., Q.L. Dai, and S.Q. Ren, *Phase transformation controlled tetragonality of MnNi-based nanocrystals*. Nanotechnology, 2016. **27**(10).
26. Shen, J., J. Li, and S.Q. Ren, *Metal-redox for MnAl-Based ternary magnetic nanocrystals*. Rsc Advances, 2016. **6**(48): p. 41781-41784.
27. Balasubramanian, B., et al., *Structure and magnetism of new rare-earth-free intermetallic compounds: Fe_{3+x}Co_{3-x}Ti₂ (0 ≤ x ≤ 3)*. Apl Materials, 2016. **4**(11).
28. Lopez-Ortega, A., et al., *Topotaxial Phase Transformation in Cobalt Doped Iron Oxide Core/Shell Hard Magnetic Nanoparticles*. Chemistry of Materials, 2017. **29**(3): p. 1279-1289.
29. Ogi, T., et al., *High-purity core-shell alpha"-Fe₁₆N₂/Al₂O₃ nanoparticles synthesized from alpha-hematite for rare-earth-free magnet applications*. Advanced Powder Technology, 2016. **27**(6): p. 2520-2525.
30. Yuzuak, G.D., E. Yuzuak, and Y. Elerman, *Hf₂Co₁₁ thin films: Rare-earth-free permanent nanomagnets*. Thin Solid Films, 2017. **625**: p. 115-121.
31. Zhao, X., et al., *Large magnetic anisotropy predicted for rare-earth-free Fe_{16-x}CoxN₂*

alloys. Physical Review B, 2016. **94**(22).

32. Pullar, R.C., *Hexagonal ferrites: A review of the synthesis, properties and applications of hexaferrite ceramics*. Progress in Materials Science, 2012. **57**(7): p. 1191-1334.

33. Rashad, M.M., et al., *Effect of Co²⁺ and Y³⁺ ions insertion on the microstructure development and magnetic properties of Ni_{0.5}Zn_{0.5}Fe₂O₄ powders synthesized using Co-precipitation method*. Journal of Magnetism and Magnetic Materials, 2015. **374**: p. 359-366.

34. Dai, Q.L., K. Patel, and S.Q. Ren, *Exchange coupled ferrite nanocomposites through chemical synthesis*. Chemical Communications, 2016. **52**(68): p. 10354-10356.

35. Dai, Q.L., et al., Solution processed MnBi-FeCo magnetic nanocomposites. Nano Research, 2016. 9(11): p. 3222-3228.

36. <http://www.allianceorg.com/pdfs/OverviewontheWorldofMagnets.pdf>

37. <http://www.duramag.com/techtalk/tech-briefs/what-is-maximum-energy-product-bhmax-and-how-does-it-correspond-to-magnet-grade/>